Proceedings Seventh Workshop Geothermal Reservoir Engineering
Stanford, December 1981. SGP-TR-55.

EXPERIMENTAL AND FINITE ELEMENT ANALYSIS OF THE STANFORD HYDROTHERMAL RESERVOIR MODEL

L.W. Swenson, Jr.
A. Hunsbedt

Stanford University
Stanford, CA 94305

Initial results are available from the first experiment to calibrate the heat extraction history of a physically simulated fractured hydrothermal reservoir using a rock loading of large, regular-shaped granite blocks. Thermocouples embedded in a set of the rock blocks and in water at various locations in the model provide heat extraction data. The data are also used to evaluate the effects of thermal stressing on heat transfer properties.

The results of the first experiment show a surprisingly uniform cross-sectional water temperature throughout the physical model indicating effective cross mixing between fracture channels. The temperature difference between rock centers and surrounding fluid reached 100°F during the cooling process, decreasing to smaller values by the end of the experiment, indicating that the rock energy extraction was relatively complete, with a high, constant temperature of the produced water.

For analysis of this and future experiments, a finite element method has been developed so that individual blocks can be represented as single elements. This approach allows less restraints on element shapes compared to finite difference models and provides possible application to full size reservoirs.

Introduction A major facet of the Stanford Geothermal Program since its inception in 1972 has been the realization that long-term commercial development of geothermal resources for electric power production will depend on optimum heat extraction from hydrothermal reservoirs. Optimum extraction is analogous to secondary and tertiary recovery of oil from petroleum reservoirs; in the geothermal case, the resource may be either heat-transfer limited or convecting-fluid limited. The effort in the Stanford Geothermal Program has been a combination of physical and mathematical modeling of heat extraction from fractured geothermal reservoirs. Experiments have included several rock loadings in the SGP physical model of a rechargeable hydrothermal reservoir, examination of thermal stressing on rock heat transfer properties, and development of mass transfer tracer methods for comparative analysis.

Although the present model predicts the overall energy extraction of the experimental reservoir quite well, it has several shortcomings with respect to modeling large scale systems. One of these was the uncertainty of axial heat conduction and heat transfer from the physical model itself.

This paper first discusses the results obtained from the Stanford Geothermal Program (SGP) physical model of a fractured hydrothermal reservoir using a rock matrix consisting of granite blocks with regular geometry. Following examination of these experimental data, concepts are introduced to extend standard finite element modeling procedures for regions experiencing steep temperature gradients and to provide a methodology for detailed investigations of extended thermal stressing on rock heat transfer properties.

Heat Extraction Experiments The SGP physical model has been described in several reports, e.g., Hunsbedt, Kruger and London (1977, 1978). The main component is a 5 ft high by 2 ft diameter insulated pressure vessel. The rock matrix used in these experiments consists of 30 granite rock blocks of 7.5" x 7.5" rectangular cross section and 24 triangular blocks as shown in Figure 1. The blocks are 10.4 inches high. The average pososity of the matrix is 17.5 percent.

Vertical channels between blocks are spaced at 0.25 inch and horizontal channels between layers are spaced at 0.17 inch. Significant vertical flow can also occur in the relatively large edge channel between the outer rock blocks and the pressure vessel.

Cold water is injected at the bottom of the vessel by a high pressure pump through a flow distribution baffle at the inlet to the rock matrix. System pressure is maintained above saturation by a flow control valve downstream of the vessel outlet. Most of the system pressure drop is in this valve while the rock matrix has essentially infinite permeability.

The water temperature is measured at the several locations shown in Figure 1: at the inlet to the vessel, the I-plane just below the baffle, the B-plane half-way up the first rock layer, the M-plane half-way up the third rock layer, the T-plane near the top of the

rock matrix, and at the vessel outlet. Temperatures were also measured at the center of four rock blocks and at two additional locations in the bottom central rock.

The rock-water-vessel system was heated to uniform initial temperature of 463±2°F, by electric strap heaters outside the vessel. The experiment was initiated by starting the injection pump and opening the flow control valve. The injection rate was constant during the experiment.

Experimental Run 5-1 has been completed with this rock matrix. Data for the experimental conditions and parameter values are summarized in Table 1.

Table 1
Experimental Data and Parameters for Run 5-1

Average Reservoir Pressure (psia)	545
Initial Reservoir Temperature (°F)	463
Final Top Temperature (°F)	312
Final Bottom Temperature (°F)	67
Injection Water Temperature (°F)	59
Initial Water Mass (lbm)	148
Injected Water Mass (lbm)	749
Water Injection Rate (lbm/hr)	150
Production Time (hr)	5

The results indicate that water temperature at the I-plane is initially slightly hotter near the surface wall due to heating by the steel. The injected water approached a uniform, constant temperature of 59°F, after about one hour. The data also show that the cross-sectional water temperatures were essentially uniform in each of the planes, with a maximum deviation of +4°F, well within the estimated uncertainty of thermocouple temperature difference of ±5°F.

Also given in Figure 2 are several representative rock center temperature transients. Comparison of these temperatures with the corresponding surrounding water temperatures showed that the maximum rock center to water temperature differences of about 100°F, developed during the cooling process decreasing to smaller values toward the end of the experiment. These data indicate that the rock energy extraction was relatively complete and the energy extracted from the rock resulted in a high, constant exit water temperature.

Data for the measured water and rock temperatures at the various thermocouple locations are given in Figure 2.

Finite Element Modeling In analyzing the heat extraction data from prior experiments in SGP physical reservoir as a one-dimensional lumped-parameter model, several problems have become evident: (1) the potential for axial heat conduction adding the need for a second-dimension in the analysis, (2) the large heat capacity of the physical model which distorts the heat transfer characteristics at the model boundaries, and (3) the need to accurately model thermal stressing effects. In order to extend the use of the lumped-parameter model to full-size geothermal reservoirs, it is desirable to remove these uncertainties in the physical model. For this purpose, a finite element heat transfer model of the present regular-shaped rock loading experiments has been developed. In this model, individual blocks can be represented as single elements. This approach allows less restraint on element shape compared to finite difference models.

The code as a general computational tool can evaluate a class of problems described by conduction or conduction-convection partial differential equations with boundary conditions consisting of specified temperature-time histories and/or specified heat flux-time histories controlled either by a direct source or by convection means. Specification of internal heat production (or loss) sources can also be included.

Some of the features of the finite-element code include: (1) free-field input of the model data; (2) automatic two- and three-dimensional block mesh generation; (3) automatic nodal renumbering to minimize the effective bandwidth; (4) line graphics presentation of the model mesh; and (5) printer and line graphics presentation of the results.

The model spatial discretization can be performed in two- or three-dimensional Cartesian coordinates or in axisymmetric cylindrical coordinates. An arbitrary number of general anisotropic material properties can be used to describe the particular reservoir being modeled. Results generated by the finite element code consist of temperature-time history curves and heat flux history curves. The data can be displayed in tables or graphically.

The development of the finite element discrete heat transfer equations begin with the governing partial differential equations given by:

$$c\frac{dT}{dt} = \nabla\cdot\underline{k}\cdot\nabla T + Q, \quad \underline{x}\in\Omega \qquad (1)$$

$$q_n = -\underline{n}\cdot\underline{k}\cdot\nabla T, \quad \underline{x}\in\Gamma_q \qquad (2)$$

$$T_s = T \qquad \underline{x}\in\Gamma_T \qquad (3)$$

where $c, T, t, \underline{k}, Q, q_n, \underline{n}$ and T_s are the material specific heat, temperature field, time, conductivity tensor, body heating source, specified normal component of heat flux, surface outward normal, and specified surface temperature, respectively. Equation (1) is the thermal equilibrium condition at each material point $\underline{x}$ in the domain Ω, while Equations (2) and (3) are the natural and essential boundary conditions, respectively.

The time derivative appearing in Equation (1) is the material time derivative,

$$\frac{d(\ )}{dt} = \frac{\partial(\ )}{\partial t} + \underline{v}\cdot\nabla(\ ) \qquad (4)$$

where, $\underline{v}$ is the velocity of the material point instantaneously positioned at the spatial point $\underline{x}$ and ∇ is the "del" vector operator with respect–to spatial coordinates. For a solid constituent $\underline{v}$ is taken to be zero while for a fluid domain $\underline{v}$ is generally non–zero. We consider the velocity field as given, being determined by previous analysis.

The discrete or weak form of Equations (1) - (3) are developed using the method of weighted residual approach. Approximating the temperature field in terms of a finite set of functions as

$$T \approx \tilde{T} = \sum_{a=1}^{q} g_a(\underline{x})\, \tau_a(t) \qquad (5)$$

and letting w_k be a generic element from a set of weighting or test functions, we use,

$$\int_{\Omega} w_k \left(c \frac{d\tilde{T}}{dt} - \underline{\nabla}\cdot\underline{k}\cdot\underline{\nabla}\tilde{T} - Q \right) d\Omega + \int_{\Gamma_q} w_k \left(q_m + \underline{n}\cdot\underline{k}\cdot\underline{\nabla}\tilde{T} \right) d\Gamma_q = 0 \qquad (6)$$

as the basis for the discretization process. Note that a constraint is placed on the approximation, Equation (5), and on the functions w_k such that $\tilde{T}(\underline{x},t) = T_s(\underline{x},t)$ and $w_k(\underline{x}) = 0$ for $\underline{x} \in \Gamma_T$.

Making use of the Green-Gauss theorem (and assuming appropriate continuity for the w_k), the second term in the domain integrand can be written as

$$-\int_{\Omega} w_k\, \underline{\nabla}\cdot\underline{k}\cdot\underline{\nabla}\tilde{T}\, d\Omega = -\int_{\Gamma_q} w_k\, \underline{n}\cdot\underline{k}\cdot\underline{\nabla}\tilde{T}\, d\Gamma_q + \int_{\Omega} \underline{\nabla} w_k \cdot \underline{k}\cdot\underline{\nabla}\tilde{T}\, d\Omega. \qquad (7)$$

Substituting (7) into (6) yields,

$$\int_{\Omega} w_k \left(c \frac{d\tilde{T}}{dt} \right) d\Omega + \int_{\Omega} \underline{\nabla} w_k \cdot \underline{k}\cdot\underline{\nabla}\tilde{T}\, d\Omega = \int_{\Omega} w_k\, Q\, d\Omega - \int_{\Gamma_q} w_k\, q_m\, d\Gamma_q. \qquad (8)$$

Finally, a choice remains to specifically identify the weighting functions w_k. We chose the Galerkin criterion and let the w_k be identified as those g_j basis functions in Equation (5) such that $g_j(\underline{x}) = 0$ for $\underline{x} \in \Gamma_T$. Substituting the approximation? and invoking the Galerkin criterion, the discretized set of heat transfer equations become,

$$[C]\{\dot{\tau}\} + [K]\{\tau\} = \{F\} \qquad (9.0)$$

where the matrix elements are given by,

$$C_{ab} = \int_{\Omega} c\, g_a\, g_b\, d\Omega \qquad (9.1)$$

$$K_{ab} = \int_{\Omega} \left(\underline{\nabla} g_a \cdot \underline{k}\cdot\underline{\nabla} g_b + c\, g_a \underline{v}\cdot\underline{\nabla} g_b \right) d\Omega \qquad (9.2)$$

$$F_a = \int_{\Omega} g_a Q\, d\Omega - \int_{\Gamma_q} g_a\, q_m\, d\Gamma_q. \qquad (9.3)$$

The convective part of K_{ab} is of course zero for solid constituents.

The evaluation of the matrix components appearing above are greatly simplified and readily computer automated by making use of finite element methodology. This approach takes the restrictions of the basis function g_k over sub-domain elements as relatively simple polynomials expressed in terms of local coordinates. Following this approach, thecomponent terms, relative to a generic element "e," can be written as

$$C^e_{ab} = \int_{\Omega^e} c\, g^e_a\, g^e_b\, d\Omega^e \qquad (10.1)$$

$$K^e_{ab} = \int_{\Omega^e} \left(\underline{\nabla} g^e_a \cdot \underline{k}\cdot\underline{\nabla} g^e_b + c\, g^e_a \underline{v}\cdot\underline{\nabla} g^e_b \right) \qquad (10.2)$$

$$F^e_a = \int_{\Omega^e} g^e_a\, Q\, d\Omega^e - \int_{\Gamma^e_q} g^e_a\, q_m\, d\Gamma^e_q \qquad (10.3)$$

where g^e_k is the restriction of g_k on the element domain Ω^e and element material boundary Γ^e_q. Global results are obtained by summing efement contributions.

Refined Element Analysis When cold water is first injected during the experiment start-up steep axial temperature gradients exist in the lower half of the physical model, see Figure 3. In addition, secondary heat extraction by cool-water reinjection will induce tensile thermal stresses in reservoir regions just below the fracture surfaces. Such stresses may result in important changes in reservoir energy extraction behavior, such as creation and growth of new cracks with additional heat transfer area and alterations in the mechanical and heat transfer properties of the rock itself. These conditions require that either a refined mesh of low order elements or a sparser mesh of high order elements be used to accurately represent the rapidly varying temperature field. Either of these modeling approaches will increase the number of problem degrees-of-freedom (DOF's), increase the analyst's modeling effort, produce longer computer runs, and lead to overall increased expenses. In an effort to achieve a balance between the requirement for high-order temperature approximation and the desire to reduce the overall number of DOF's, a condensed super-element methodology was used.

Consider a super-element, defined as an assembly of many simpler elements, as shown schematica11y below.

$$\{\tau\} = \begin{Bmatrix} \underline{\tau}^E \\ \underline{\tau}^I \end{Bmatrix} \qquad (11)$$

The temperature parameters $\underline{\tau}$ can be considered partitioned into two sets, one containing the "exterior" parameters $\underline{\tau}^E$ and the second containing the "interior" parameters $\underline{\tau}^I$. In like manner the super-element thermal equilibrium equations can be partitioned and written as

$$\begin{bmatrix} \underline{C}^{EE} & \underline{C}^{EI} \\ \underline{C}^{IE} & \underline{C}^{II} \end{bmatrix} \begin{Bmatrix} \dot{\underline{\tau}}^E \\ \dot{\underline{\tau}}^I \end{Bmatrix} + \begin{bmatrix} \underline{K}^{EE} & \underline{K}^{EI} \\ \underline{K}^{IE} & \underline{K}^{II} \end{bmatrix} \begin{Bmatrix} \underline{\tau}^E \\ \underline{\tau}^I \end{Bmatrix} = \begin{Bmatrix} \underline{F}^E \\ \underline{F}^I \end{Bmatrix} \qquad (12)$$

Reduction of the total number of DOF's is effected in two parts. Constraint conditions among the τ^E set can be written as

$$\tau^E = (G)\,\tau^{\hat{E}} \qquad (13)$$

where (G) is a matrix of constants relating the total exterior set τ^E in terms of a subset of τ^E, $\tau^{\hat{E}}$, which are to be retained in the analysis.

Secondly, constraint conditions among the τ^I set is taken to be of the form

$$\tau^I = (S)\,\eta \qquad (14$$

where (S) is a matrix of numbers and η is a vector of generalized time dependent coordinates. While the analyst is at liberty to select (S) in any manner deemed appropriate, a seemingly natural choice is to choose the columns of (S) as certain eigenvectors of the generalized eigenvalue problem

$$\left([K^{II}] - \alpha_k [C^{II}]\right) S_k = 0 . \qquad (15)$$

Here, α_k is the k^{th} eigenvalue associated with the k^{th} eigenvector S_k. Physically, S_k can be identified as an approximation to the k^{th} thermal eigenfunction associated with the continuum interior of the super-element domain while α_k is an approximation to the associated characteristic diffusivity.

Finally reduction of the super-element equations, Equation (12), is performed using the transformation

$$\begin{Bmatrix} \tau^E \\ \tau^I \end{Bmatrix} = \begin{pmatrix} G & 0 \\ 0 & S \end{pmatrix} \begin{Bmatrix} \tau^{\hat{E}} \\ \eta \end{Bmatrix} \qquad (16)$$

and congruent transformations, leading to

$$\begin{bmatrix} C^{\hat{E}\hat{E}} & C^{\hat{E}N} \\ C^{N\hat{E}} & C^{NN} \end{bmatrix} \begin{Bmatrix} \dot{\tau}^{\hat{E}} \\ \dot{\eta} \end{Bmatrix} + \begin{bmatrix} K^{\hat{E}\hat{E}} & K^{\hat{E}N} \\ K^{N\hat{E}} & K^{NN} \end{bmatrix} \begin{Bmatrix} \tau^{\hat{E}} \\ \eta \end{Bmatrix} = \begin{Bmatrix} F^{\hat{E}} \\ F^{N} \end{Bmatrix} \qquad (17$$

where the condensed super-element submatrices in this equation are given by

$$C^{\hat{E}\hat{E}} = G^T C^{EE} G , \quad K^{\hat{E}\hat{E}} = G^T K^{EE} G \qquad (18.1-.2)$$

$$C^{\hat{E}N} = G^T C^{EI} S , \quad K^{\hat{E}N} = G^T K^{EI} S \qquad (18.3-.4)$$

$$C^{N\hat{E}} = S^T C^{IE} G , \quad K^{N\hat{E}} = S^T K^{IE} G \qquad (18.5-.6)$$

$$C^{NN} = S^T C^{II} S , \quad K^{NN} = S^T K^{II} S \qquad (18.7-.8)$$

$$F^{\hat{E}} = G^T F^E \;\&\; F^N = S^T F^N . \qquad (18.9-.10)$$

It should be noted that with proper scaling of the eigenvectors S_k, the submatrices C^{nn} and K^{nn} are the identity matrix, I and the diagonal matrix of associated eigenvalues, respectively.

DISCUSSION The results of the first experiment using the large, regular-shaped granite blocks indicates that the attempt to calibrate the spatial time-temperature history of the loading will be successful. Several additional experiments are planned with larger injection flow rates to produce "heat transfer limited" reservoir conditions, in which substantial rock-water temperature differences exist throughout the transient. Such conditions should result in a much more rapid exit water temperature decrease.

In the completed experiment, the observed cross-sectional water temperatures were relatively uniform even with the relatively large flow area at the edge channels between the rock loading and the vessel. Possible explanations of this apparent uniform cross-sectional water temperature, inter-block channel area, include: (1) relative magnitudes of the heat available at the various channels; (2) relative pressure drops in each channel; and (3) cross mixing between channels.

Estimates of the heat transfer from around the edge channels (including heat from the steel vessel) compared to the inter-block channels were about 1.65, not quite as large as the flow area ratio of 2.07. Thus, the edge channels may be lower in temperature than the inter-block channels. The perforated flow distribution baffle at the bottom of the vessel has been shown to be sufficiently efficient in providing uniform flow entering the rock matrix below the lowest rock layer. Channel to channel pressure drop differences are not expected to be sufficiently large to affect the average channel flow velocities at the mean flow rate of only 5 ft/hr. The most likely reason for the observed uniform water temperatures appears to be the energy exchange between channels due to mass transfer. This aspect of the analysis warrants further observations in the future experiments and in the analysis.

Examination of the experimental data clearly indicate that steep axial temperature gradients exist in the lower half of the physical model. The maximum spatial axial temperature gradient varies with time, being largest at the start of the experiment and slowly decreasing as the experiment progresses. In addition, the physical location of the peak axial temperature gradient starts at the base of the rock pile and gradually moves upward. Significant temperature variations were also measured within the individual granite blocks; temperature differences between the center of the blocks and the surrounding fluid measured as much as 100°F.

Observation of these temperature gradients in the water and in the individual blocks has motivated the development of a refined finite element methodology. The approach developed for analysis of the physical chimney model uses a super-element technique with certain imposed constraints to reduce the overall degrees-of-freedom. Super-element DOF reduction was

generalized by separating the external constraints relations from the internal constraint relations. This separation of constraint equations permits the analyst considerable flexibility in approximating the super-element "surface" temperature field and the "internal" temperature field to a degree that is deemed appropriate for each. Initial experience has shown that refined super-elements perform well in regions where steep fluid and rock temperature gradients exist and hold promise for efficient hydro-thermal finite element analysis.

REFERENCES

Hunsbedt, A., P. Kruger, and A.L. London, "Recovery of Energy from Fracture-Stimulated Geothermal Reservoirs," Journal of Petroleum Technology, August 1977.

Hunsbedt, A., P. Kruger, and A.L. London, "Laboratory Studies of Fluid Production from Artificially Fractured Geothermal Reservoirs," Journal of Petroleum Technology, May 1978.

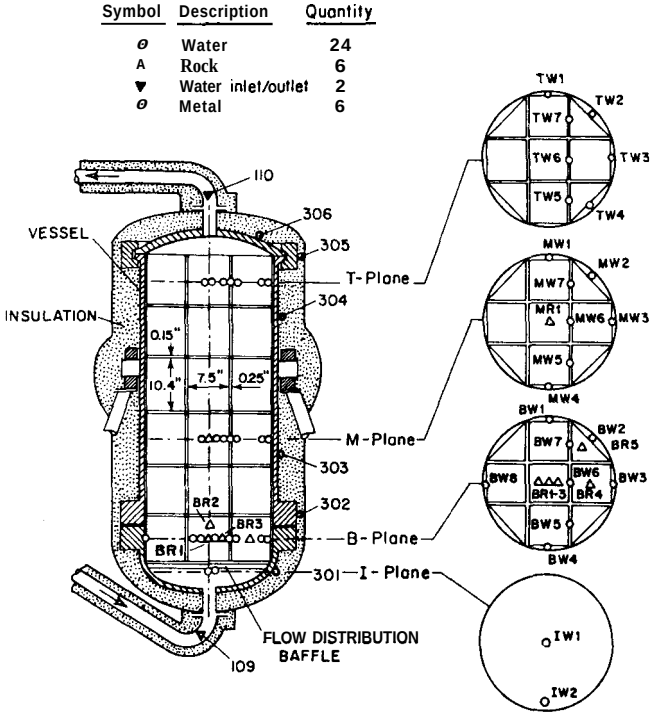

Figure 1. Experimental Rock Matrix Configuration and Thermocouple Locations.

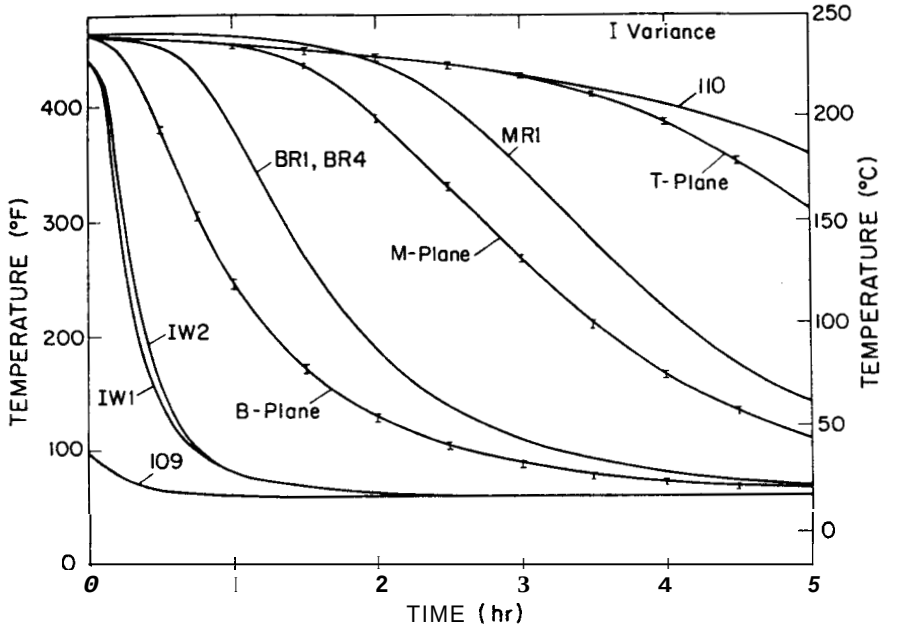

Figure 2. Water and Rock Temperatures as Functions of Time

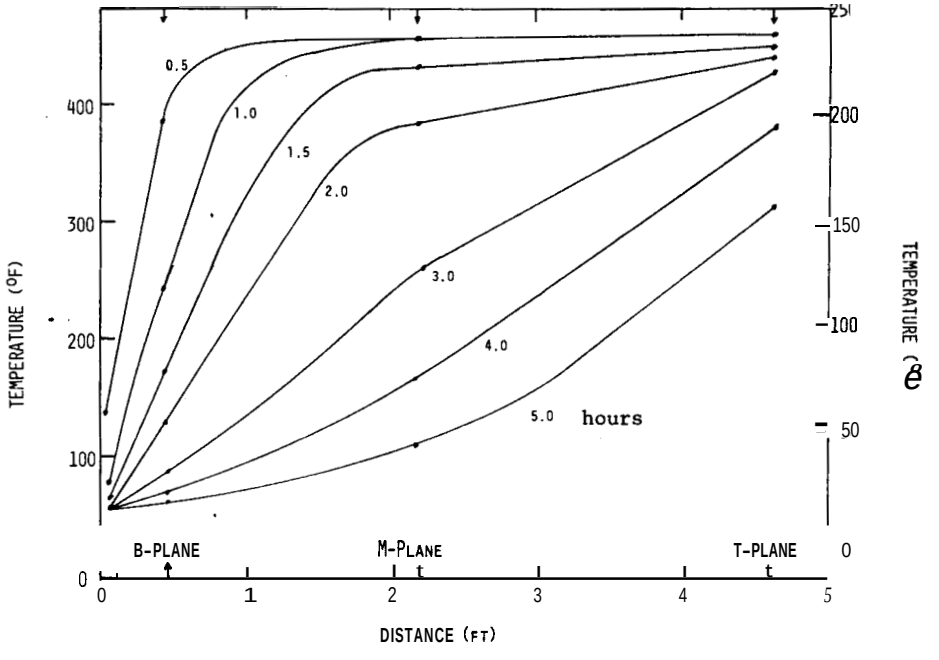

Figure 3. Isochronal Water Temperature Distributions